Research Square

Preprints are preliminary reports that have not undergone peer review.
They should not be considered conclusive, used to inform clinical practice,
or referenced by the media as validated information.

Large inter-model variations in the future subpolar North Atlantic hydrodynamics from CMIP6 simulations

Anne Britt Sando

anne.britt.sando@imr.no

Institute of Marine Research: Havforskningsinstituttet https://orcid.org/0000-0002-2373-2808

Andreas Born

University of Bergen: Universitetet i Bergen

Research Article

Keywords: AMOC, SPG, Poleward Transport, North Atlantic circulation, CMIP6

Posted Date: March 30th, 2026

DOI: https://doi.org/10.21203/rs.3.rs-9139454/v1

License: This work is licensed under a Creative Commons Attribution 4.0 International License.
Read Full License

Large inter-model variations in the future subpolar North Atlantic hydrodynamics from CMIP6 simulations

Anne Britt Sandø *[1,3] and Andreas Born[2,3]

[1]Department of Oceanography and Climate, Institute of Marine Research, Bergen, Norway
[2]Department of Earth Science, University of Bergen, Bergen, Norway
[3]Bjerknes Centre for Climate Research, Bergen, Norway

Abstract

Driven by the ongoing debate on the potential consequences of a future Atlantic Meridional Overturning Circulation (AMOC) collapse for the Nordic Seas and their marine ecosystems, this study examines the relationship between different patterns in the North Atlantic across various CMIP6 models and scenarios. Under the high-emission SSP5-8.5 scenario, all models show a weakened AMOC associated with increased heat transport into the Nordic Seas across the Iceland-Scotland Ridge (ISR). While ISR temperature trends vary across CMIP6 models, with both positive and negative trends, volume transport overcompensates for negative temperature trends, resulting in consistently positive heat transport trends.

In contrast to short-term variability in the present day climate where AMOC seems to have lagged response to atmospheric forcings such as wind and atmosphere-ocean heat fluxes, the different long-term AMOC responses in a warmer future appear to be decisive for different trends in subpolar temperatures and corresponding shifts in temperature gradients and wind stress curl patterns. The increased northward volume transport across the ISR ridge seems partly caused by this south-eastward shift in the wind stress curl, giving rise to stronger southerly winds west of the British Isles, and partly as a function of increased freshwater in the North Atlantic and along the eastern rim of the Nordic Seas

Due to negative temperature trends of different strength in the subpolar gyre and ISR across the SSP scenarios, the Nordic Seas are projected to experience less warming in SSP5-8.5 than in SSP3-7.0 by the end of the century. The highly different results from models and scenarios with respect to climate exposures indicate large uncertainties, with additional uncertainties in risk reports about climate impacts on the marine ecosystem that complicate decision-makers' actions to minimize future damage.

Keywords: AMOC, SPG, Poleward Transport, North Atlantic circulation, CMIP6

1 Introduction

The inflow of Atlantic Water from the North Atlantic Ocean to the Nordic Seas across the Iceland-Scotland Ridge (ISR, Figure 1) is of major importance to the regional climate in Nordic countries due to the $\sim$ 300 TW transport of heat into the Nordic and Arctic Seas (Østerhus *et al.*, 2005) and covaries with an atmospheric pattern resembling the North Atlantic Oscillation (Nilsen *et al.*, 2003; Sandø *et al.*, 2012; Asbjørnsen *et al.*, 2021). Along the rim of the Nordic Seas, warm Atlantic Water is gradually transformed to dense water by ocean-atmosphere heat loss and freshwater gain (Mauritzen, 1996; Eldevik *et al.*, 2009). Finally, the dense waters leave the Nordic Seas through deep channels in the Faroe-Shetland-Channel (Hansen and Østerhus, 2000) and Denmark Strait (Macrander *et al.*, 2005) and enters the lower limb of the Atlantic Meridional Overturning Circulation (AMOC) in the North Atlantic.

The AMOC plays a significant role in the global climate system, and its behavior in a warming climate is a matter of significant concern (Weijer *et al.*, 2022) due to a potential collapse (Liu *et al.*, 2017; Boers, 2021; Ditlevsen and Ditlevsen, 2023) when approaching a tipping point (McKay *et al.*, 2022; van Westen *et al.*, 2024; Rahmstorf, 2024). On the other side, observed Atlantic sea surface temperatures (SST) and pre-industrial control runs from the Coupled Model Intercomparison Project Phase 6 (CMIP6) models show a prevalence of natural AMOC variability since 1900, and that the 1 Sv decrease after 1980 is in the range of internal multidecadal variability (Latif *et al.*, 2022). On decadal timescales, changes in AMOC are primarily related to buoyancy anomalies in a western transition zone along the boundary between the subtropical and subpolar gyres (Buckley and Marshall, 2016), but recent research increasingly emphasizes the importance of the Nordic Seas

*Corresponding author: anne.britt.sando@imr.no

and Arctic Mediterranean for the AMOC (Årthun *et al.*, 2023). Despite global warming, parts of the subpolar gyre region (SPG) in the North Atlantic ocean have been observed to cool (Fox *et al.*, 2022). The emergence of this cooling, has been linked to reduced ocean heat transport into the region of cooling as a consequence of a slowdown of the AMOC, and to increased ocean heat transport out of the region into higher latitudes (Nummelin *et al.*, 2017; Keil *et al.*, 2020).

To project how climate in the SPG and Nordic Seas may evolve in future warming, it is of great importance to understand the relationship between large-scale ocean dynamics in the North Atlantic and the ocean heat transport across the ISR. Here, the objective is to investigate this relationship by analyzing different CMIP6 models to increase our understanding of factors that account for the temporal and inter-model variability in both past and future periods from Historical and Shared Socioeconomic Pathways (SSP) scenario simulations.

2 Method

To study this relationship, we calculate indices and/or spatial trends for the following: the northern limb of AMOC, the strength of the SPG circulation, heat fluxes between the atmosphere and ocean (HFAO), the wind stress curl (WSC), and the mixed layer depth (MLD), all for the same area covering the SPG. In addition, we analyze indices for temperature at the core of the Atlantic Water (T), and heat- and volume transports (HT, VT) at the ISR. This study builds on the analysis by Madonna and Sandø (2022), but due to the improvement of the evaluated characteristics from CMIP5 to CMIP6, the focus is here on CMIP6 models only. Modeled data from CMIP6 is downloaded from the Earth System Grid Federation (ESGF) (Cinquini *et al.*, 2014). The analysis is based on monthly data covering the period 1850-2014 and 2015-2100 (SSP5-8.5), and with the ensemble member r1i1p1f1 from 5 CMIP6-models. In addition, 4 scenarios (SSP1-2.6, SSP2-4.5, SSP3-7.0 and SSP5-8.5) from the Norwegian Earth System Model (NorESM2; Seland *et al.* (2020)) are analyzed to study the inter-scenario spread. The decimal numbers in the scenario types describe the additional radiative forcing in year 2100 compared to the pre-industrial baseline, namely 2.6, 4.5, 7.0 and 8.5 Wm^{-2}. Only models that provide necessary variables for calculation of the indices of interest are included.

2.1 North Atlantic indices

Figure 1 illustrates the areas and sections of interest where the indices are calculated. The AMOC index is calculated as the time series of the maximum Ocean Meridional Overturning Mass Streamfunction ($msftmz$) or Ocean Y Overturning Mass Streamfunction ($msftyz$) north of about 40° N in the North Atlantic.

The index for the SPG circulation stength is calculated in two different ways; the minimum of the Barotropic Streamfunctiom (BT) and the first principle component from an Empirical Orthogonal Function analysis of the sea surface height (SSH_{EOF}) in a SPG limited by 48 and 64° N and -60 and -1° E. The BT index is then the time series of the maximum Ocean Barotropic Mass Streamfunction ($msftbarot$) in the above defined SPG (Figure 1), and the SSH_{EOF} index is the first principle component of the Empirical Orthogonal Function of the detrended the Sea Surface Height Above Geoid (zos). The reason for using two different ways to represent the variability of the horizontal circulation is the various descriptions and applications of the SPG-index in the literature (Häkkinen and Cavalieri, 1989; Hátún *et al.*, 2005; Foukal and Lozier, 2017; Hátún and Chafik, 2018; Koul *et al.*, 2020). Also, the mean Historical BT downloaded from the ESGF might have been calculated differently (IPSL-CM6A-LR, MPI-ESM1-2-HR) so that BT along the coast is different from 0.

Indices for HFAO and MLD in the SPG are calculated as area-weighted averages of Downward Heat Flux at Sea Water Surface ($hfds$) and Ocean Mixed Layer Thickness Defined by Sigma T ($mlotst$), respectively, and over the same area as BT and SSH_{EOF}. Spatial trends for the WSC are calculated as function of the Surface Downward Eastward Wind Stress ($tauu$) and Surface Downward Northward Wind Stress ($tauv$). The vertical component of the wind stress curl is

$$\mathrm{WSC} = \frac{\partial \tau_y}{\partial x} - \frac{\partial \tau_x}{\partial y} \tag{1}$$

Similarly, spatial trends for sea salinity and temperature are calculated as function of the Sea Water Salinity (so) and Sea Water Temperature ($thetao$).

2.2 Iceland-Scotland Ridge indices

As described in Madonna and Sandø (2022), we calculate monthly HT and VT from the model outputs (hfx, hfy) and (umo, vmo), and consider the ISR (Figure 1), which encompasses the Iceland-Faroe Ridge and the Faroe-Scotland Channel. hfx and hfy (umo and vmo) contain all contributions to x- and y-ward heat (mass) transport from resolved and parameterized processes. Volume transports are calculated from mass transports

assuming a density of water of 1000 kg m^{-3}. This assumption can lead to a slight (< 3 %) overestimation of VT but it does not affect the variability (Madonna and Sandø, 2022).

For each section, we find grid indices that are closest to specific geographic positions at each end of the section, and we also check that the endpoints are on land as the resolution and the corresponding bathymetry differ from model to model. Thereafter, we find the grid indices and corresponding x and y transport components for each grid cell along a line between the two endpoints to calculate the total HT and VT across the considered sections. For each model, we use the temperature at 100 m depth as an estimation for the Atlantic Water core temperature, and calculate temperature at ISR, T, along the same sections as for HT and VT.

2.3 Correlation and trend calculations

To investigate relationships between indices, their time series are correlated with each other after smoothing the time series. All correlations and regressions are done on monthly time series which are detrended and deseasoned by detrending of each calendar month separately. The effective degrees of freedom are found according to Chelton (1983), i.e. taking into consideration the autocovariance of all time series. Significance levels are calculated by the standard Student's t-test, using $\alpha = 0.05$ (5% significance level). Projected changes during the scenarios are based on the trends in time series multiplied by the length of the period between 2015 and 2100, where trends are calculated by least-squares fitting a first order polynomial.

3 Literature based model evaluations

Of the 7 CMIP6 models studied in Madonna and Sandø (2022), only 5 models have all variables needed for both the Historical period and the SSP-scenario in this analysis. In the following section we have included short literature based evaluations of these models that is relevant for the region and processes of interest.

3.1 IPSL-CM6A-LR

Over-stratification in the ocean appears to limit deep ocean warming and affects upper ocean heat content trends in IPSL-CM6A-LR historical simulations (Boucher *et al.*, 2020). The model has been flagged for a weak AMOC response (Palmer *et al.*, 2023) in some assessments, which affects North Atlantic temperature and sea surface biases. This includes a warm winter bias in parts of the Arctic ((Boucher *et al.*, 2020)), and even though improved from earlier model versions, sea ice extent and seasonal cycles remain imperfect (Boucher *et al.*, 2020), likely tied to biases in temperature and ocean heat uptake. Furthermore, the poleward volume and heat transports into the Nordic Seas are too high compared to observational estimates (Madonna and Sandø, 2022).

3.2 MPI-ESM1-2-HR

Broad CMIP6 performance diagnostics frequently find that MPI-ESM1-2-HR performs reasonably within ensemble distributions for near-surface meteorological fields (2 m temperature, specific humidity, winds) (Pan *et al.*, 2025). Particularly relevant for this study, MPI-ESM1-2-HR performs very well with respect to inflowing water characteristics to the Nordic Seas (Madonna and Sandø, 2022). Some studies also place MPI-ESM1-2-HR in the better performing category for certain regions or variables (e.g., seasonal wind patterns), but divergent performance in others (e.g., deep ocean thermodynamics, precipitation) implies the model is not uniformly superior across all climate diagnostics (Pan *et al.*, 2025). In focused evaluations in climatic gateways (e.g., Arctic gateways), MPI-ESM1-2-HR can display cold biases in the colder air mass regimes (Pithan *et al.*, 2025), as well as in the inflowing waters to the Barents Sea (Madonna and Sandø, 2022).

3.3 MRI-ESM2-0

The basic model evaluation shows that MRI-ESM2-0 reasonably reproduces the mean climate state and interannual variability, but the model overestimates mid-20th century cooling and subsequent warming relative to observations in historical simulations, indicating a modest bias in reproducing observed temperature changes over the twentieth century (YUKIMOTO *et al.*, 2019). There are cold biases in high-latitude winter conditions (Pithan *et al.*, 2025), and for the poleward inflow to the Nordic Ses, MRI-ESM2-0 underestimates temperature, but overestimates heat and volume transports (Madonna and Sandø, 2022). MRI-ESM2-0 generally performs well in near-surface atmospheric fields relative to some models, but deep ocean temperature and salinity fields remain challenging and show significant spread among CMIP6 models (Pan *et al.*, 2025).

3.4 NorESM2

In multi-model evaluations, NorESM2-MM often emerges as a relatively well-performing model for integrated fields (Pan *et al.*, 2025), and similarly to MPI-ESM1-2-HR, NorESM2 performs very well with respect to inflowing water characteristics to the Nordic Seas (Madonna and Sandø, 2022). However, regional temperature biases exist, and cold biases in polar regions result in too strong meridional gradient and greater sea ice area than observations in some seasons, and lower than observed in others (Seland *et al.*, 2020). Surface winds and storm tracks show also systematic circulation biases with tropospheric zonal winds that tend to be too westerly in parts of the extratropics, and with storm-track intensity that may be underestimated in regions such as the Norwegian and Barents Seas (Seland *et al.*, 2020).

4 Results

4.1 Mechanism for variability in Historical period

MPI-ESM1-2-HR, NorESM1-MM, and NorESM1-LM match observations of HT and VT within uncertainty, and likewise IPSL-CM5A-LR, NorESM2-MM, and NorESM2-LM agree with the observed mean AMOC at OSNAP (Table 1). From the overall evaluation of both AMOC in the OSNAP section (Lozier, 2023) and heat and volume transports at the ISR (Madonna and Sandø, 2022), we find that the family of NorESM2 models is closest to the observed values (Table 1), while MPI-ESM1-2-HR is similarly close to ISR observed transports. The increase in HT by 33 TW in NorESM2-MM is somewhat less that the estimated increase of about 50 TW (from +150 to +200 TW) for the entire Greenland-Scotland Ridge section over the last century (Smedsrud *et al.*, 2022), but the model agrees with the observation that this increase is primarily due to enhanced volume transport rather than increased temperature. IPSL-CM6A-LR is in clear contradiction with the observational evidence because of its clear negative trend in VT, compensated by a strong T increase, resulting in a similar HT trend as in the other models.

The left hand panel in Figure 2 shows time series and trends for some of the indices of interest (AMOC, BT, HT, T and VT) during the Historical period from 1850 to 2014. The AMOC is relatively stable with small positive trends in all models (up to 2.5 Sv over the historical period), except MPI-ESM1-2-HR which has a negative trend corresponding to a decrease of slightly less than 1 Sv during the same period (Figure 2a). The BT trends are all positive with changes up to 12 Sv, except the NorESM2s which are weakly negative (Figure 2b).

Correlations are calculated based on monthly timeseries with a running-mean filter of 12 months and represent variability on interannual time scales (Table 2). The time lags in the correlations vary widely, with almost no lag between different transports to very variable lags between the indices in the SPG and indices at the ISR. NorESM2-MM and NorESM2-LM show in general relatively high correlations between AMOC, BT and SSH_{EOF} (Table 2). Small, but significant positive correlations between VT and AMOC with negative time lags indicate that higher VT leads higher AMOC with up to about 3 years.

The significant negative correlations between HT and HFAO in the SPG with a lag of 1 month in 4 out of 5 models (Table 2) (0 month lag with no running-mean filter) indicate with a strong degree of uncertainty that increased ocean-atmosphere heat losses in the SPG barely lead increased heat transports across the ISR. Similarly, significant negative correlations between AMOC and HFAO in the same region with a lag of 24-53 months indicate that increased AMOC lags the deceased HFAO (increased ocean-atmosphere heat losses) by about 2-4 years.

4.2 Variability and trends in future scenario SSP5-8.5

A similar analysis has been performed for the future scenario SSP5-8.5 from year 2015 to 2100. The corresponding time series and trend lines of the modeled indices together with the change versus mean are shown in Figure 2, and the correlations are given in Table 3. The correlations for the future scenario are in general less significant partly due to shorter time series, but some correlations are strengthened and apply to most models for correlations between HT and VT. NorESM2-LM has the highest number of significant correlations, and these are relatively similar to the Historical period. In addition, this model has now obtained a significant correlation between T and SSH which indicates that variability in SSH leads T at ISR with more than 4 years.

While the AMOC trends in the Historical period are relatively small with a mix of positive and negative numbers, the trends during the SSP5-8.5 scenario are all strongly negative compared to the Historical period in all models, with a decrease in the range ∼5-18 Sv (Figure 2a). Similarly, the minimum BT in the SPG tend to increase (become weaker) during the future scenario, with exception of MPI-ESM1-2-HR which decreases slightly (becomes stronger) (Figure 2b). With respect to HT, 3 of 5 analyzed models, MRI-ESM2-0, IPSL-CM6A-LR and MPI-ESM1-2-HR, have strong increases (∼100-150 TW), while HT in NorESM2-MM and NorESM2-LM is relatively unchanged (Figure 2c). These trends reflect to large extent the VT in the same section (Figure 2e), but they are modified by strongly opposite T trends, i.e. positive trends in IPSL-CM6A-LR and MPI-ESM1-2-HR

and negative trends in MRI-ESM2-0, NorESM2-MM and NorESM2-LM (Figure 2d). Also, the model with the strongest decrease in AMOC, MRI-ESM2-0, has the strongest decrease in T, and vise versa for IPSL-CM6A-LR.

To analyse the mechanism behind the diverging temperatures at ISR at the core of the Atlantic Water, we consider the spatial distribution of temperature change at 100 m in the North Atlantic (Figure 3, right), upstream of ISR. The different panels clearly show opposite temperature changes in SPG; increasing in IPSL-CM6A-LR and MPI-ESM1-2-HR, and decreasing in MRI-ESM2-0, NorESM2-LM and NORESM2-MM. The trends of colder SPG water in MRI-ESM2-0 and the NorESM2s are also associated with strong positive trends in heat flux from the atmosphere to the ocean (Figure 3), left), and a decrease in MLD (Figure 4, right). Furthermore, the model with the largest heat transport trend into the Nordic Seas (MPI-ESM1-2-HR, Figure 2c) has the smallest reduction in the overturning north of about 60° N (Figure 5) along with the strongest increase in MLD in the Greenland Sea and a relatively moderate decrease in the Norwegian and Barents Sea compared to the other models (Figure 4).

Since the increase in HT is largely due to the increase in VT (Madonna and Sandø, 2022), we study the changes that could cause this dynamic change. Figure 5 (left) shows that all models have increased barotropic cyclonic circulation (more negative BT) in the Nordic Seas and over the Greenland-Scotland Ridge. The role of winds on this circulation is illustrated by the WSC in Figure 4, left). The WSC is reduced in the SPG and increased in the eastern North Atlantic between 48°N and 60°N, reflecting the gradients in the changed temperature pattern (Figure 3). Also changes in salinity can alter the circulation as a result of the baroclinic pressure gradient that arises from horizontal salinity gradients. The resulting plots of sea surface salinity (SSS) in Figure 6 (left) show that there is a relatively strong west-east salinity gradient across the Nordic Seas, with a freshwater anomaly along the eastern coastal shelf inn all models, especially in MRI-ESM2-0.

4.3 NorESM2-MM scenario differences

To see how AMOC and temperature are linked in different scenarios, we have chosen to study four scenarios of NorESM2-MM. Figure 7 shows the 0-200m depth-averaged temperature trends in the four scenarios SSP1-2.6, SSP2-4.5, SSP3-7.0 and SSP5-8.5. In the Norwegian and Barents Seas, the positive trends increase from SSP1-2.6 to SSP3-7.0 in both strength and extent, while there is a corresponding increase in the negative trends from SSP3-7.0 to SSP5-8.5 in the SPG and slightly north of the ISR. Similarly, Figure 8 shows time series of temperature at 0-200m in the northeastern SPG and in different areas in the Norwegian and Barents Seas together with time series of AMOC, HT and VT. The AMOC strength decreases with higher SSP scenario (higher radiative forcing), and so does the temperature in the northeastern SPG, except that SSP3-7.0 has a decrease similar to SSP1-2.6. SSP3.7-0 is the outlayer also for temperature changes north of ISR, where it has the strongest increase of all scenarios. This corresponds well to HT in SSP3-7.0 which by far has the strongest increase.

5 Discussion

5.1 Historical period

The long list of correlations between indices in Table 2 shows a variety of significant correlations and corresponding lags, and some of them, such as the ones between heat and volume transports, are high as expected. The highest number of significant correlations are found for the best evaluated models; namely MPI-ESM1-2-HR (8), NorESM2-MM (11) and NorESM2-LM (16).

Significant negative correlations between atmosphere-ocean heat fluxes in the SPG and heat transports at ISR at short time lags indicate that winds in the SPG is a common denominator for both ocean-atmosphere heat flux variability (Alexander and Scott, 1997) in the SPG and for transports across the ISR as winds south of Iceland have been shown to drive variability in transports across ISR (Madonna and Sandø, 2022). Such a wind driven relationship for the variable inflows to the Nordic Seas was also found in Sandø *et al.* (2012) where the atmospheric pattern resembled the North Atlantic Oscillation, and where the inflow through the Faroe-Shetland Channel led to an immediate barotropic response on both the light outflow and dense overflow in the Denmark Strait. Furthermore, Langehaug *et al.* (2012) found a strong relationship between the SPG strength and the overflow in the Denmark Strait, where the overflow leads SPG circulation strength by 1 year, supporting our lagged relationships between transports and barotropic streamfunction of about 1-2 years. This is consistent with the theoretical understanding based on idealized modeling (Born and Stocker, 2014).

The significant correlations with somewhat longer time lags of up to about 4 years between transports and AMOC also allows a contribution from advection of hydrodynamic anomalies around the rim of the Nordic Seas which have been shown to take about 3 years from the ISR to the Denmark Strait (Eldevik *et al.*, 2009). Processes involving water mass transformation and overturning in the Nordic Seas may therefore play a significant role in driving the exchanges across the Greenland-Scotland Ridge (Hansen and Østerhus, 2000) and further downstream in the North Atlantic, in addition to similar deepwater formation processes in the SPG.

5.2 Future scenario

The simulated heat transport across the ISR separates the CMIP6 models in this study into two groups for the SSP5-8.5 scenario, two models that show virtually no change, and three that simulate a similar increase. However, the reason behind the increase is not uniform across the models as two of the three with an increase also exhibit a clear temperature increase in the source region together with a weak to moderate increase in volume transport, while the third pairs a strong cooling with a marked increase in volume transport. To be discussed here is therefore i) the cause of the different temperature trends in the ISR and ii) the cause of the different volume transport trends in the same region.

The AMOC plays a central role in climate through its northward heat and freshwater transports (Buckley and Marshall, 2016). According to Figure 5, MRI-ESM2-0 has the strongest reduction in AMOC, followed by NorESM2-MM and NorESM2-LM, which lead to less northward transport of warm Atlantic Water in the North Atlantic compared to IPSL-CM6A-LR and MPI-ESM1-2-HR. The resulting distribution of negative temperature trends at 100 m and at surface in the SPG region can be seen in Figures 3 and 6 (right). A clear sign of the socalled cold blob (Keil *et al.*, 2020), is spread over a large area in the subpolar North Atlantic in MRI-ESM2-0, NorESM2-MM and NorESM2-LM, explaining the opposite temperature trends at ISR at the rim of the cold blob.

The positive trends in the ISR volume transport in all models seem to be partly caused by a shift in the positive WSC from its present day position in the SPG southeastwards towards the British Isles, illustrated by a negative trend developing in the SPG region and a positive trend west of the British Isles (Figure 4, left). An increased WSC west of the British Isles (48-60°N) is in agreement with Köhler *et al.* (2025) who find that there is a southward shift of the upper-level jet stream primarily driven by the change in the meridional temperature gradient. Observation based results from satellite-era reanalysis products indicate that there is a general trend of a poleward shift in the jet stream due to the amplified Arctic warming (Wood *et al.*, 2003), but the warming trend in the North Atlantic is in the opposite direction due to the emerging cold blob in the subpolar region (Figure 3), and the corresponding WSC is therefore shifted southwards there (Figure 4, left). The variability of large-scale horizontal circulation in the North Atlantic and into the Nordic Seas is in the present day climate mainly driven by winds in the form of wind stress at the surface which in turn leads to changes in surface elevation and associated barotropic and baroclinic pressure gradients (Nilsen *et al.*, 2003; Sandø *et al.*, 2012). Here, long-term changes in the WSC show a relatively strong increase in the North Atlantic west of the British Isles in most models (Figure 4). Based on both observational and modeling studies, a strong WSC at 55°N is associated with a stronger North Atlantic Oscillation and greater inflow to the Nordic Seas at the ISR (Orvik and Skagseth, 2003; Sandø and Furevik, 2008). The increased ISR transports and barotropic cyclonic circulation in the Nordic Seas, which is a common feature in all models, therefore appear to be influenced by a shifted WSC, particularly in MRI-ESM2-0, but also by increased estuarine and/or melt water circulation as a function of increased freshwater in the North Atlantic and along the eastern rim of the Nordic Seas (Figure 6).

All models in this study show reduced MLD in the eastern subpolar gyre and over the ISR into the Norwegian Sea, illustrating the role of this region in production of dense waters in the present day climate (Lozier, 2023), and vice versa in a warmer climate as in SSP5-8.5 (Figure 4, right). Also, using global climate models Årthun *et al.* (2023) show that a future strengthening of the Nordic Seas density-space overturning circulation may be due to enhanced horizontal circulation and a strengthened zonal density gradient. They also find that the simulated changes in this overturning circulation is a clear link to large scale redistribution of sea surface temperatures.

5.3 NorESM2-MM scenario differences

In the four NorESM2-MM scenarios studied here, it is interesting to see how the different amounts of cold water in the North Atlantic impact the temperatures in the Nordic Seas, so that SSP3-7.0 ends up with stronger positive temperature trends than the SSP5-8.5 scenario, especially in the Norwegian Sea. Despite negative SPG temperature trends in all scenarios, reflecting different rates of AMOC decline, positive volume transport trends at ISR cause a clear positive heat transport trend in SSP3-7.0 and a marginally positive one in SSP5-8.5.

Although models analyzed in this study are consistent with observations that there are no strong trends in ISR volume and heat transports, or temperature in the recent past (Orvik, 2022), they suggest that such consequences of global warming can materialize in the coming decades, with cooling in subpolar region in 3 of 5 models. Future temperature reductions of up to 5.5°C partly support studies that claim that high emissions of greenhouse gases will result in a strongly reduced AMOC and corresponding temperature reductions in the northern North Atlantic and neighboring areas (Vellinga and Wood, 2002; Bellomo et al., 2021). It should be noted though that the reduced temperatures in NorESM2s are limited to an area close to the ISR, and that the ocean temperatures north of this cold blob are increasing. Such warming is different from the overall cooling in the Nordic Seas with the strongly reduced AMOC shown in Liu *et al.* (2017), although the length of our simulations are relatively short compared to their multi-century long simulations of doubled CO_2 concentrations

with nudging to observed salinities.

5.4 Uncertainties

An objective in climate modeling is to produce realistic results for the past, present and future climate. Despite different skills to reproduce observed mean values for AMOC, and transports and temperature at ISR, the different models herein all agree that there will be an increase in heat transport across the ISR in SSP5-8.5. Whether this is correct or not, remains to be seen, but there are observation based results supporting a similar, but weaker trend for the last century (Smedsrud *et al.*, 2022). That said, it is not sufficient that the models are right with respect to such a trend, they must also be right for the right reason. The opposing trends in temperature at ISR that are compensated by trends in volume transport of different strengths to produce positive trends in heat transport reveal that some models tend to be right for the wrong reason. As described in Section 3, the models have different degrees of climate sensitivity, biases in poleward transport, temperature and deep thermodynamics. In the following, we will briefly discuss our results in regard to past model evaluations in the region interest.

IPSL-CM6A-LR has a realistic AMOC for present day climate, but it has been flagged for a weak AMOC response (Palmer *et al.*, 2023). The model also has a weak future AMOC reduction compared to the other models, and the evolution of the cold blob is therefore very limited. Too high poleward volume transport in combination with the relatively high and increasing North Atlantic temperature entail high and increasing poleward heat transport also in the future. Despite realistic MPI-ESM1-2-HR poleward temperature, volume, and heat transport for today's climate (Madonna and Sandø, 2022), the model produces too high an AMOC, and since the rate of future AMOC reduction is similar to that of IPSL-CM6A-LR and weak compared to MRI-ESM2-0 and NorESM2s, MPI-ESM1-2-HR ends up with the highest AMOC at the end of this century. Differently from MRI-ESM2-0 that has far too high present day AMOC, too high poleward volume- and heat transports, and too low temperature at ISR, NorESM-LM and NorESM-MM score well on all these characteristics. Yet these 3 models end up with roughly the same low value of AMOC and an associated reduction in temperature in the North Atlantic. Regardless of similar ocean characteristics in the two NorESM2s, the future volume transport is somewhat bigger in NorESM2-MM than in NorESM2-LM, possibly due to the different trends in WSC. The only difference between the two models lies in the resolution of the atmospheric component, which may explain a different atmospheric response to slowly evolving gradients in the ocean.

Furthermore, an analysis by Chylek *et al.* (2024) reveals, based on an evaluation of Arctic warming between the periods 1960-1991 and 2014-2023, that not all CMIP6 models are equally representative for future scenarios. Only 7 of the 19 models simulate the Arctic warming within ±15% of the observed value. Only 2 models, IPSL-CM6A-LR and NorESM2-LM, of our 5 models were represented in that study, where NorESM2-LM happened to be within ±15% of the observed value, while IPSL-CM6A-LR was above. NorESM2-LM was also 1 of only 3 models that are within the ±15% observed value for both the Arctic and global temperature. For the future SSP2-4.5 simulation, NorESM2-LM underestimates the future Arctic warming compared to the average of seven models identified within ±15% of the observed warming, but is considerably closer to this mean than IPSL-CM6A-LR which overestimate the same average future Arctic warming. This is in agreement with the record high IPSL-CM6A-LR surface warming among models in this study. The underestimated Arctic warming in NorESM2-LM also fits well with the findings regarding low AMOC and poleward transports at the end of this century.

This study focus on the hydrodynamic impacts of different AMOC trends and not specifically on the reason for the different AMOC trends, but according to Sgubin *et al.* (2017), many CMIP5 models underestimate the chance of future abrupt SPG cooling due to systematic model biases and varying capability in simulating the present-day stratification in the SPG. Deep ocean temperature and salinity fields also remain challenging with significant spread among CMIP6 models (Pan *et al.*, 2025). So, how different model biases relate to the AMOC climate response is still unclear, but the AMOC response in a warmer future seems to be decisive for the subpolar temperature trends and corresponding shifts in WSC as a function of the shifted temperature gradients in the ocean. The interpretation of the highly different temperature trends at ISR should therefore be made with these results in mind. This is particularly important in risk analyzes on future climate change and associated effects on marine ecosystems as subsequent consequences of these different trends on sea ice extent and primary production, and cascading effects on higher trophic levels, can contribute to large uncertainties (Hare *et al.*, 2016; Kjesbu *et al.*, 2021; Sandø *et al.*, 2024; Myksvoll *et al.*, 2023)

6 Conclusions

We have here studied the relationship between various indices related to circulation and northward heat transport in different CMIP6 models and different future scenarios. For the present climate, CMIP6 models show that winds south of Iceland have a strong and immediate effect on heat and volume transports into the Nordic

Model	Ocean resolution	HT [TW]	VT [Sv]	AMOC [Sv]
IPSL-CM6A-LR	362x332	326.6	6.5	15.3±2.8
MPI-ESM1-2-HR	802x404	239.7	3.7	21.0±2.8
MRI-ESM2-0	360x363	303.7	6.7	23.7±3.2
NorESM2-LM	360x385	227.3	3.1	15.7±2.2
NorESM2-MM	360x385	234.6	3.7	15.5±2.0
Observations		231±43	3.4 ±1.4	16.7±0.6

Table 1: CMIP6 models, their associated horizontal ocean resolution in terms of longitudinal and latitudinal grid points, their respective net heat (HT (TW)) and volume (VT (Sv)) transports at the Iceland-Scotland Ridge (ISR) for the period 1986-2005, and AMOC north of 40° N (Sv). Observation-based estimate of AMOC is from OSNAP at 53-60° N (Lozier, 2023), and estimates of HT and VT are based on observations as described in Madonna and Sandø (2022)

.

Seas. These transports also covary with atmosphere-ocean heat fluxes in the SPG, and AMOC a few years later. Additionally, inter-annual variability in ISR heat and volume transport leads corresponding changes in barotropic circulation strength in the SPG, which subsequently influences AMOC variability.

Under the high-emission SSP5-8.5 scenario, all models show a weakened AMOC associated with increased heat transport into the Nordic Seas. While ISR temperature trends vary across CMIP6 models, with both positive and negative numbers, volume transport trends overcompensates for negative temperature trends, resulting in consistently positive heat transport trends.

In contrast to short-term variability in the present climate, where AMOC seems to have lagged response to atmospheric forcings such as winds and atmosphere-ocean fluxes, AMOC appears to be decisive for long-term trends in subpolar temperatures and corresponding shifts in the temperature gradients and WSC patterns in a warmer future scenario. The increased northward volume transport across the ISR ridge seems to be driven by this south-eastward shift in the WSC, giving rise to stronger southerly winds west of the British Isles, but altered freshwater distribution in the North Atlantic and Nordic Seas may also contribute to increased transports into the Nordic Seas. Also, due to negative temperature trends of different strength in the SPG and ISR across the SSP scenarios, the Nordic Seas are projected to experience less warming in SSP5-8.5 than in SSP3-7.0 by the end of the century.

The highly different results from models and scenarios with respect to climate exposures therefore indicate large uncertainties, with additional uncertainties in risk reports about climate impacts on the marine ecosystem that complicate decision-makers' actions to minimize future damage.

Acknowledgement

We acknowledge the World Climate Research Programme's Working Group on Coupled Modelling, which is responsible for CMIP, and we thank the climate modeling groups listed in Table 1 for producing and making available their model output. We also acknowledge storage space from the Norwegian National e-Infrastructure for Research Data (NIRD, #NS9034K), and finally Geir Ottersen for fruitful discussions.

Statements and Declarations

This work was funded by the Bjerknes Centre for Climate Research through the SKD projects DYNASOR and O2Ocean, and by the EU project SEACLIM. The authors have no relevant financial or non-financial interests to disclose. Both authors contributed to the study conception and design. Material preparation, data collection and analysis were performed by Anne Britt Sandø. The first draft of the manuscript was written by Anne Britt Sandø and both authors commented on previous versions of the manuscript. Both authors read and approved the final manuscript.

Data Availability

The datasets analysed during the current study are available in the Earth System Grid Federation (ESGF) repository, https://aims2.llnl.gov/search/cmip6.

	MPI-HR	NorESM-M	NorESM-L	IPSL-LR	MRI
AMOC-BT	-0.42@13	-0.62@6	-0.62@4	-	-
AMOC-HFAO	-	-0.35@25	-0.35@24	-	-0.32@53
AMOC-SSH	-	-0.59@19	-0.68@17	-	-
BT-HFAO	-	-	0.36@18	-	
BT-SSH	-	0.56@5	0.56@9	-	-
HT-AMOC	0.39@-39	-	0.39@-12		
HT-BT	-	-0.41@-14	-0.34@-11	-	-
HT-HFAO	0.25@-22	-0.35@1	-0.35@1	-0.33@1	-0.36@1
HT-SSH	-0.44@-5	-	-	-	0.40@-6
HT-T	0.63@-1	0.57@1	-0.28@30	0.49@-1	0.35@-3
HT-VT	0.77@1	0.84@0	0.84@0	0.73@0	0.80@0
T-AMOC	-	0.36@66	0.40@58	-	-
T-BT	-	-	0.31@-13	-	-
T-HFAO	-	-	0.21@8	-	-
T-SSH	-0.49@69	0.34@19	-	-	-
VT-AMOC	0.38@-42	0.55@-51	0.54@-13	-	-
VT-BT	-0.40@-28	-0.57@-18	-0.53@-12	-	-0.30@-29
VT-SSH	-	-48@-3	-0.51@-3	-0.36@-2	0.36@-4
VT-T	-	-	-	-	-

Table 2: Significant correlations between different indices at the ISR and in the subpolar North Atlantic for MPI-ESM1-2-HR, NorESM2-MM, NorESM2-LM, IPSL-CM6A-LR and MRI-ESM2-0 simulations covering the Historical period from 1850-2014. AMOC, BT, HT, SSH, T and VT are abbreviations for Atlantic meridional Overturning circulation north of 40° N (Sv), Barotrophic Streamfunction (Sv), ocean Heat Transport (TW), first principle component of the Empirical Orthogonal Function of the Sea Surface Height (m), Temperature at 100m (°C) and ocean Volume Transport (Sv), respectively. A running-mean filter of 12 months is applied to the time series. Positive/negative signs of the number denoted after @ means that the first index lag/lead the second by the specified number.

	MPI-HR	NorESM-M	NorESM-L	IPSL-LR	MRI
AMOC-BT	-	-	-0.61@0	-	-
AMOC-HFAO	-	0.41@0	-0.33@17	-	-
AMOC-SSH	-	-	-0.65@-34	-	-
BT-HFAO	-	-	-	-	-
BT-SSH	-	-	-	-	-
HT-AMOC	-	-	-	-	-
HT-BT	-	-	-	-	-
HT-HFAO	-	-0.43@1	-0.32@1	-0.45@2	-
HT-SSH	-	-	-	-	-
HT-T	-	-	-	-	-
HT-VT	0.95@0	0.90@0	0.93@0	0.85@0	0.78@0
T-AMOC	-	-	-	-	-
T-BT	-	-	-	-	-
T-HFAO	-	-	-0.35@40	0.42@29	-
T-SSH	-	-	-0.59@53	-	-
VT-AMOC	-	0.49@-13	-	-	-
VT-BT	-	-	-	-	-
VT-SSH	-	-	-	-	-
VT-T	-	-	-	-	-

Table 3: As Table 2, but for SSP5-8.5.

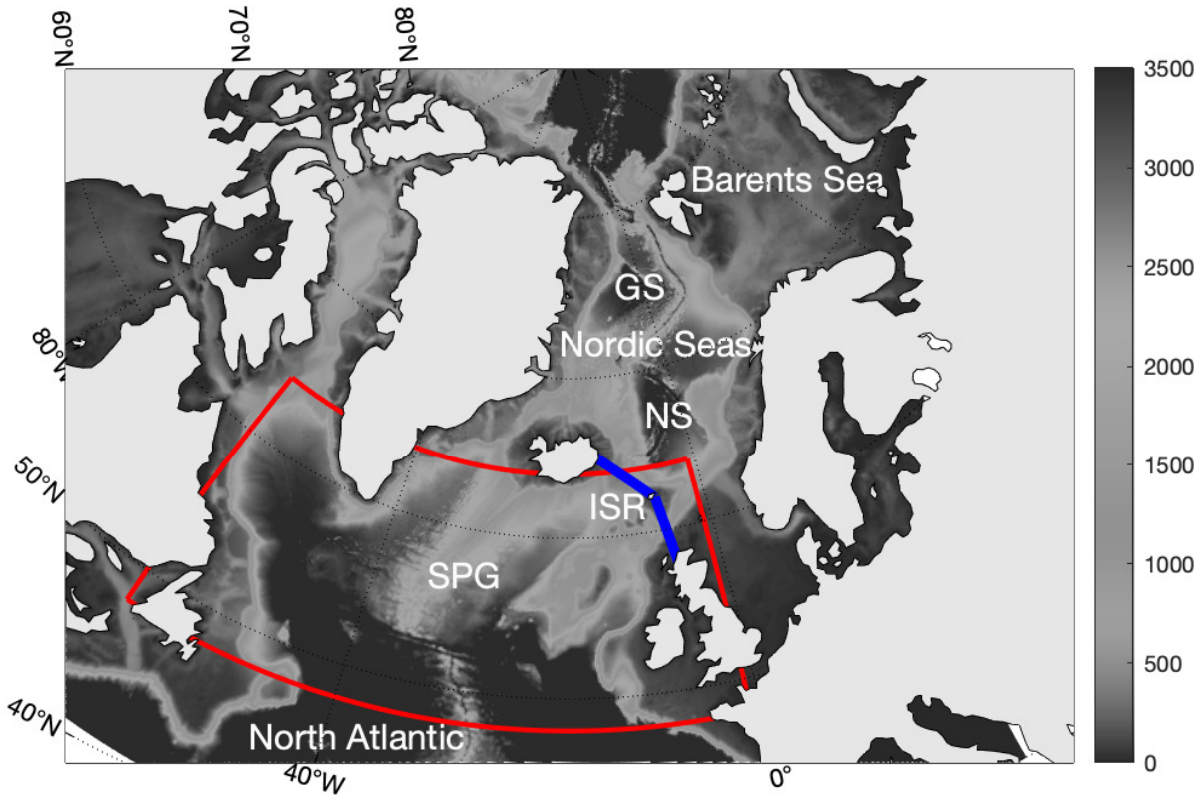


Figure 1: Bathymetric map (m) with the subpolar gyre region (SPG) and the Iceland-Scotland Ridge (ISR) in which indices are calculated. GS and NS are abbreviations for Greenland Sea and Norwegian Sea, respectively.

References

Alexander, M. A. and Scott, J. D. 1997. Surface flux variability over the north pacific and north atlantic oceans. iJournal of Climate, 10.

Årthun, M., Asbjørnsen, H., Chafik, L., Johnson, H. L., and Våge, K. 2023. Future strengthening of the nordic seas overturning circulation. Nature Communications, 14: 2065. URL https://doi.org/10.1038/s41467-023-37846-6.

Asbjørnsen, H., Johnson, H. L., and Årthun, M. 2021. Variable nordic seas inflow linked to shifts in north atlantic circulation. Journal of Climate, 34: 7057 – 7071. URL https://journals.ametsoc.org/view/journals/clim/34/17/JCLI-D-20-0917.1.xml.

Boers, N. 2021. Observation-based early-warning signals for a collapse of the atlantic meridional overturning circulation. Nature Climate Change, 11: 680–688. URL https://doi.org/10.1038/s41558-021-01097-4.

Born, A. and Stocker, T. F. 2014. "Two Stable Equilibria of the Atlantic Subpolar Gyre. Journal of Physical Oceanography, 44: 246 – 264. URL https://journals.ametsoc.org/view/journals/phoc/44/1/jpo-d-13-073.1.xml.

Boucher, O., Servonnat, J., Albright, A. L., Aumont, O., Balkanski, Y., Bastrikov, V., Bekki, S., *et al.* 2020. Presentation and evaluation of the ipsl-cm6a-lr climate model. Journal of Advances in Modeling Earth Systems, 12: e2019MS002010. URL https://agupubs.onlinelibrary.wiley.com/doi/abs/10.1029/2019MS002010. E2019MS002010 10.1029/2019MS002010.

Buckley, M. W. and Marshall, J. 2016. Observations, inferences, and mechanisms of the atlantic meridional overturning circulation: A review. Reviews of Geophysics, 54: 5–63. URL https://agupubs.onlinelibrary.wiley.com/doi/abs/10.1002/2015RG000493.

Chelton, D. B. 1983. Effects of sampling errors in statistical estimation. Deep Sea Research Part A, 30.

Chylek, P., Folland, C. K., Klett, J. D., Wang, M., Lesins, G., and Dubey, M. K. 2024. Why does the ensemble mean of cmip6 models simulate arctic temperature more accurately than global temperature? Atmosphere, 15. URL https://www.mdpi.com/2073-4433/15/5/567.

Cinquini, L., Crichton, D., Mattmann, C., Harney, J., Shipman, G., Wang, F., Ananthakrishnan, R., *et al.* 2014. The Earth System Grid Federation: An open infrastructure for access to distributed geospatial data. Future Generation Computer Systems, 36: 400–417.

Ditlevsen, P. and Ditlevsen, S. 2023. Warning of a forthcoming collapse of the atlantic meridional overturning circulation. Nature Communications, 14: 4254. URL https://doi.org/10.1038/s41467-023-39810-w.

Eldevik, T., Nilsen, J. E. Ø., Iovino, D., Olsson, K. A., Sandø, A. B., and Drange, H. 2009. Observed sources and variability of Nordic seas overflow. Nature Geoscience, 22: 1–9.

Foukal, N. P. and Lozier, M. S. 2017. Assessing variability in the size and strength of the north atlantic subpolar gyre. Journal of Geophysical Research: Oceans, 122: 6295–6308. URL https://agupubs.onlinelibrary.wiley.com/doi/abs/10.1002/2017JC012798.

Fox, A. D., Handmann, P., Schmidt, C., Fraser, N., Rühs, S., Sanchez-Franks, A., Martin, T., *et al.* 2022. Exceptional freshening and cooling in the eastern subpolar north atlantic caused by reduced labrador sea surface heat loss. Ocean Science, 18: 1507–1533. URL https://os.copernicus.org/articles/18/1507/2022/.

Häkkinen, S. and Cavalieri, D. J. 1989. A study of the oceanic heat fluxes in the Greenland, Norwegian and Barents Seas. J. Geoph. Res., 95: 6145–6157.

Hansen, B. and Østerhus, S. 2000. North Atlantic-Nordic Seas exchanges. Prog. Oceanog., 45: 109–208.

Hare, J. A., Morrison, W. E., Nelson, M. W., Stachura, M. M., Teeters, E. J., Griffis, R. B., Alexander, M. A., *et al.* 2016. A vulnerability assessment of fish and invertebrates to climate change on the northeast U.S. continental shelf. PLOS ONE, 11: 1–30. URL https://doi.org/10.1371/journal.pone.0146756.

Hátún, H., Sandø, A. B., Drange, H., Hansen, B., and Valdimarsson, H. 2005. Influence of the Atlantic Subpolar Gyre on the Thermohaline Circulation. Science, 309: 1841–1844.

Hátún, H. and Chafik, L. 2018. On the recent ambiguity of the north atlantic subpolar gyre index. Journal of Geophysical Research: Oceans, 123: 5072–5076. URL https://agupubs.onlinelibrary.wiley.com/doi/abs/10.1029/2018JC014101.

Keil, P., Mauritsen, T., Jungclaus, J., Hedemann, C., Olonscheck, D., and Ghosh, R. 2020. Multiple drivers of the north atlantic warming hole. Nature Climate Change, 10: 667–671.

Kjesbu, O. S., Sundby, S., Sandø, A. B., Alix, M., Hjøllo, S., Tiedemann, M., Skern-Mauritzen, M., *et al.* 2021. Highly mixed impacts of near-future climate change on stock productivity proxies in the north east Atlantic. Fish and Fisheries, n/a. URL https://onlinelibrary.wiley.com/doi/abs/10.1111/faf.12635.

Köhler, D., Räisänen, P., Naakka, T., Nordling, K., and Sinclair, V. A. 2025. The future north atlantic jet stream and storm track: relative contributions from sea ice and sea surface temperature changes. Weather and Climate Dynamics, 6: 669–694. URL https://wcd.copernicus.org/articles/6/669/2025/.

Koul, V., Tesdal, E., J., Bersch, M., Hátún, H., Brune, S., Borchert, L., *et al.* 2020. Unraveling the choice of the north Atlantic subpolar gyre index. Scientific reports, 10.

Langehaug, H. R., Medhaug, I., Eldevik, T., and Otterå, O. H. 2012. Arctic/atlantic exchanges via the subpolar gyre. Journal of Climate, 25: 2421–2439.

Latif, M., Sun, J., Visbeck, M., and Hadi Bordbar, M. 2022. Natural variability has dominated atlantic meridional overturning circulation since 1900. Nature Climate Change, 12: 455–460. URL https://doi.org/10.1038/s41558-022-01342-4.

Liu, W., Xie, S.-P., Liu, Z., and Zhu, J. 2017. Overlooked possibility of a collapsed atlantic meridional overturning circulation in warming climate. Science Advances, 3: e1601666. URL https://www.science.org/doi/abs/10.1126/sciadv.1601666.

Lozier, M. S. 2023. Overturning in the subpolar north atlantic: a review. Philosophical Transactions of the Royal Society A: Mathematical, Physical and Engineering Sciences, 381: 20220191. URL https://royalsocietypublishing.org/doi/abs/10.1098/rsta.2022.0191.

Macrander, A., Send, U., Valdimarsson, H., Jónsson, S., , and Kase, R. H. 2005. Interannual changes in the overflow from the Nordic Seas into the Atlantic Ocean through Denmark Strait. Geophysical Research Letters, 32: 1–4.

Madonna, E. and Sandø, A. B. 2022. Understanding differences in north atlantic poleward ocean heat transport and its variability in global climate models. Geophysical Research Letters, 49: e2021GL096683. URL https://agupubs.onlinelibrary.wiley.com/doi/abs/10.1029/2021GL096683. E2021GL096683 2021GL096683.

Mauritzen, C. 1996. Production of dense overflow waters feeding the north atlantic across the greenland-scotland ridge. part 1: Evidence for a revised circulation scheme. Deep Sea Research Part I: Oceanographic Research Papers, 43: 769–806. URL https://www.sciencedirect.com/science/article/pii/0967063796000374.

McKay, D. I. A., Staal, A., Abrams, J. F., Winkelmann, R., Sakschewski, B., Loriani, S., Fetzer, I., *et al.* 2022. Exceeding 1.5°c global warming could trigger multiple climate tipping points. Science, 377: eabn7950. URL https://www.science.org/doi/abs/10.1126/science.abn7950.

Meccia, V. L., Iovino, D., and Bellucci, A. 2021. North atlantic gyre circulation in primavera models. Climate Dynamics, 56: 4075–4090. URL https://doi.org/10.1007/s00382-021-05686-z.

Myksvoll, M. S., Sandø, A. B., Tjiputra, J., Samuelsen, A., Çağlar Yumruktepe, V., Li, C., Mousing, E. A., *et al.* 2023. Key physical processes and their model representation for projecting climate impacts on subarctic atlantic net primary production: A synthesis. Progress in Oceanography, 217: 103084. URL https://www.sciencedirect.com/science/article/pii/S0079661123001271.

Nilsen, J. E. Ø., Gao, Y., Drange, H., Furevik, T., and Bentsen, M. 2003. Simulated North Atlantic - Nordic Seas water mass exchanges in an isopycnic coordinate OGCM. Geophysical Research Letters, 30: 1536.

Nummelin, A., Li, C., and Hezel, P. J. 2017. Connecting ocean heat transport changes from the midlatitudes to the arctic ocean. Geophysical Research Letters, 44: 1899–1908.

Orvik, K. A. 2022. Long-term moored current and temperature measurements of the atlantic inflow into the nordic seas in the norwegian atlantic current; 1995–2020. Geophysical Research Letters, 49: e2021GL096427.

Orvik, K. A. and Skagseth, Ø. 2003. The impact of the wind stress curl in the North Atlantic on the Atlantic inflow to the Norwegian Sea toward the Arctic. Geophysical Research Letters, 30: 1884.

Østerhus, S., Turrell, W. R., Jónsson, S., and Hansen, B. 2005. Measured volume, heat, and salt fluxes from the Atlantic to the Arctic Mediterranean. Geophysical Research Letters, 32: L07603.

Palmer, T. E., McSweeney, C. F., Booth, B. B. B., Priestley, M. D. K., Davini, P., Brunner, L., Borchert, L., *et al.* 2023. Performance-based sub-selection of cmip6 models for impact assessments in europe. Earth System Dynamics, 14: 457–483. URL https://esd.copernicus.org/articles/14/457/2023/.

Pan, X., Liu, C., Wang, Z., Xu, Z., Liang, X., and Li, X. 2025. Evaluating the performance of cmip6 models in the southern temperate zone with a multivariable integrated evaluation method. Frontiers in Marine Science, Volume 12 - 2025. URL https://www.frontiersin.org/journals/marine-science/articles/10.3389/fmars.2025.1651187.

Pithan, F., Naumann, A. K., and Maturilli, M. 2025. Too cold, too saturated? evaluating climate models at the gateway to the arctic. Atmospheric Chemistry and Physics, 25: 3269–3285. URL https://acp.copernicus.org/articles/25/3269/2025/.

Rahmstorf, S. 2024. Is the atlantic overturning circulation approaching a tipping point? Oceanography. URL https://doi.org/10.5670/oceanog.2024.501.

Sandø, A. B. and Furevik, T. 2008. The relation between the wind stress curl in the North Atlantic and the Atlantic inflow to the Nordic Seas. J. Geoph. Res., 113.

Sandø, A. B., Nilsen, J. E. Ø., and Eldevik, T. 2012. Mechanisms behind the Nordic Seas-North-Atlantic exchanges. J. Geoph. Res., 117.

Sandø, A. B., Hjøllo, S. S., Hansen, C., Skogen, M. D., Hordoir, R., and Sundby, S. 2024. A multi-scenario analysis of climate impacts on plankton and fish stocks in northern seas. Fish and Fisheries, 25: 711–732. URL https://onlinelibrary.wiley.com/doi/abs/10.1111/faf.12834.

Seland, Ø., Bentsen, M., Olivié, D., Toniazzo, T., Gjermundsen, A., Graff, L. S., Debernard, J. B., *et al.* 2020. Overview of the Norwegian Earth System Model (NorESM2) and key climate response of CMIP6 DECK, historical, and scenario simulations. Geoscientific Model Development, 13: 6165–6200. URL https://gmd.copernicus.org/articles/13/6165/2020/.

Sgubin, G., Swingedouw, D., Drijfhout, S., Mary, Y., and Bennabi, A. 2017. Abrupt cooling over the north atlantic in modern climate models. Nature Communications, 8: 14375. URL https://doi.org/10.1038/ncomms14375.

Smedsrud, L. H., Muilwijk, M., Brakstad, A., Madonna, E., Lauvset, S. K., Spensberger, C., Born, A., *et al.* 2022. Nordic seas heat loss, atlantic inflow, and arctic sea ice cover over the last century. Reviews of Geophysics, 60: e2020RG000725. URL https://agupubs.onlinelibrary.wiley.com/doi/abs/10.1029/2020RG000725. E2020RG000725 2020RG000725.

van Westen, R. M., Kliphuis, M., and Dijkstra, H. A. 2024. Physics-based early warning signal shows that amoc is on tipping course. Science Advances, 10: eadk1189. URL https://www.science.org/doi/abs/10.1126/sciadv.adk1189.

Weijer, W., Haine, T. W., Siddiqui, A. H., Cheng, W., Veneziani, M., and Kurtakoti, P. 2022. Interactions between the arctic mediterranean and the atlantic meridional overturning circulation: A review. Oceanography. URL https://doi.org/10.5670/oceanog.2022.130.

Wood, R. A., Vellinga, M., and Thorpe, R. 2003. Global warming and thermohaline circulation stability. The Royal Society, 361: 1961–1975.

YUKIMOTO, S., KAWAI, H., KOSHIRO, T., OSHIMA, N., YOSHIDA, K., URAKAWA, S., TSUJINO, H., *et al.* 2019. The meteorological research institute earth system model version 2.0, mri-esm2.0: Description and basic evaluation of the physical component. Journal of the Meteorological Society of Japan. Ser. II, 97: 931–965.

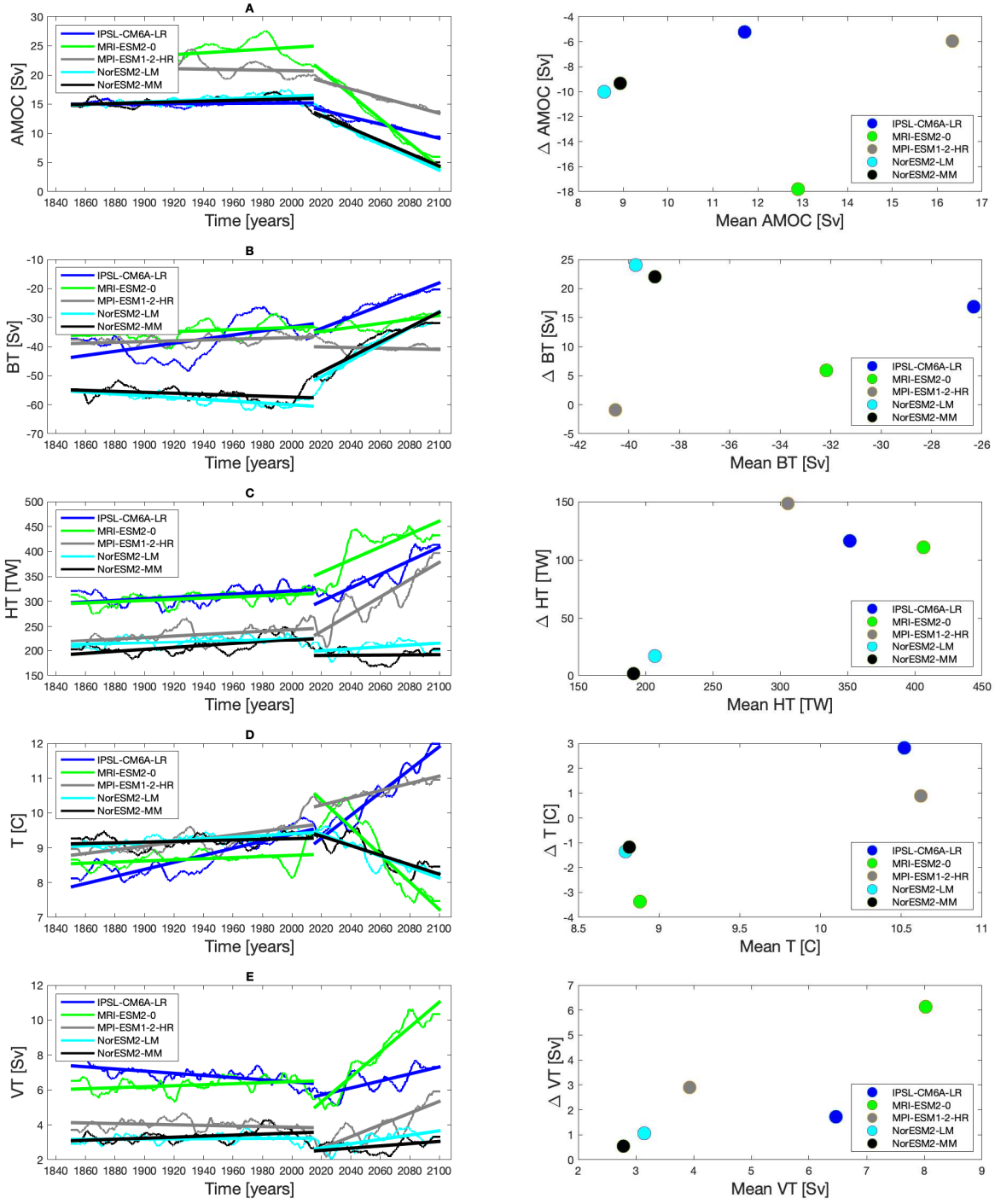


Figure 2: Time series and trends (Historical and SSP5-8.5, left) and change versus mean (SSP5-8.5, right) for Atlantic meridional overturning cirulation (AMOC) north of 40° N (Sv), barotropic streamfunction (BT) (Sv) in SPG, and ISR heat transport (HT) (TW), ISR temperature at 100 m depth (T) (°C) and ISR volume transport (VT) (Sv) (top-down).

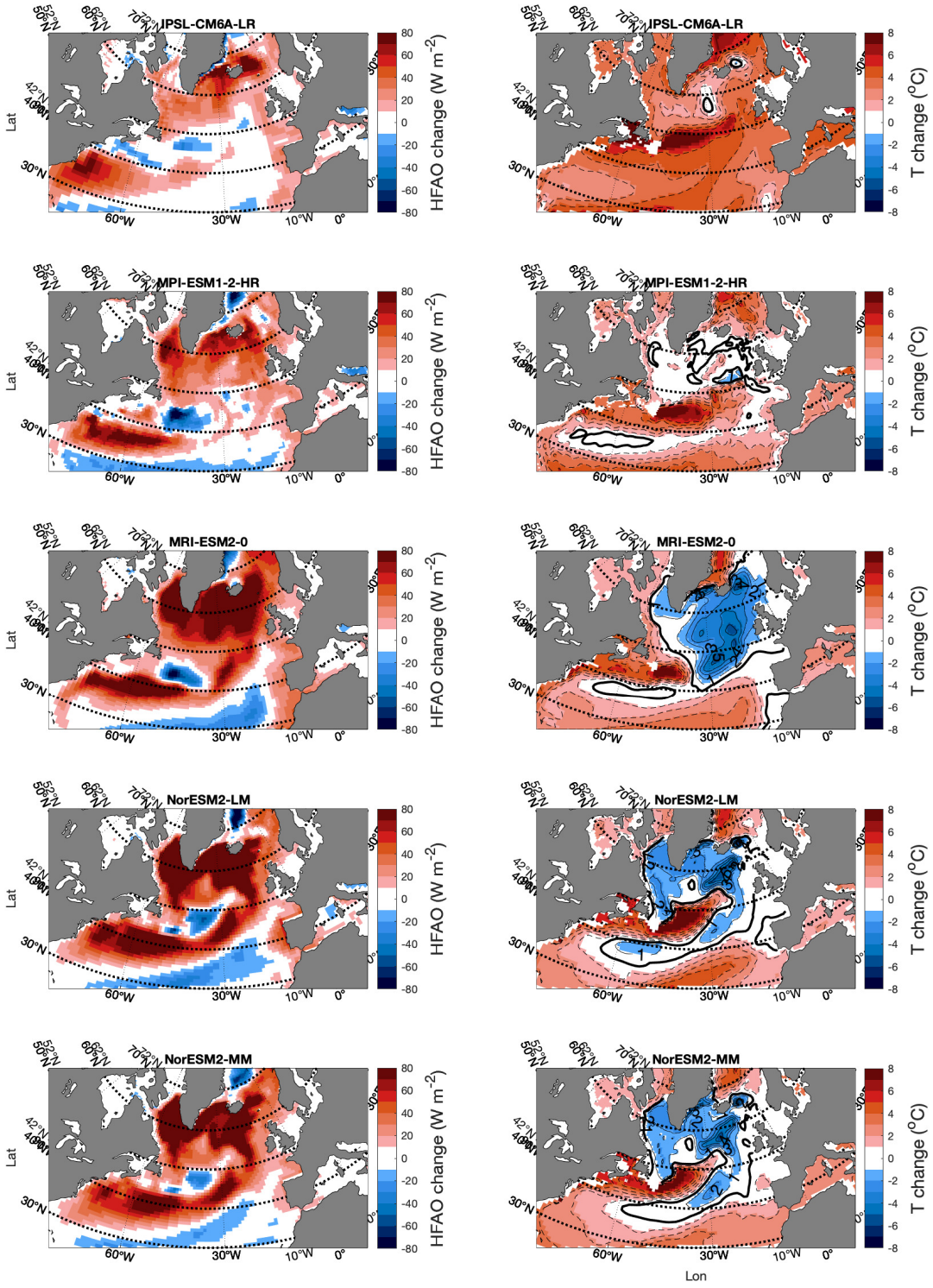


Figure 3: Spatial changes in the atmosphere-ocean heatflux (HFAO) (Wm^{-2}, left) and temperature at 100 m (°C, right) for IPSL-CM6A-LR, MPI-ESM1-2-HR, MRI-ESM2-0, NorESM2-LM and NorESM2-MM (top-down) between 2015 and 2100. The contours in the panel to the right show the difference between temperature at 100 m and at surface (T_{100}-SST). The the thick contour is the 0-contour.

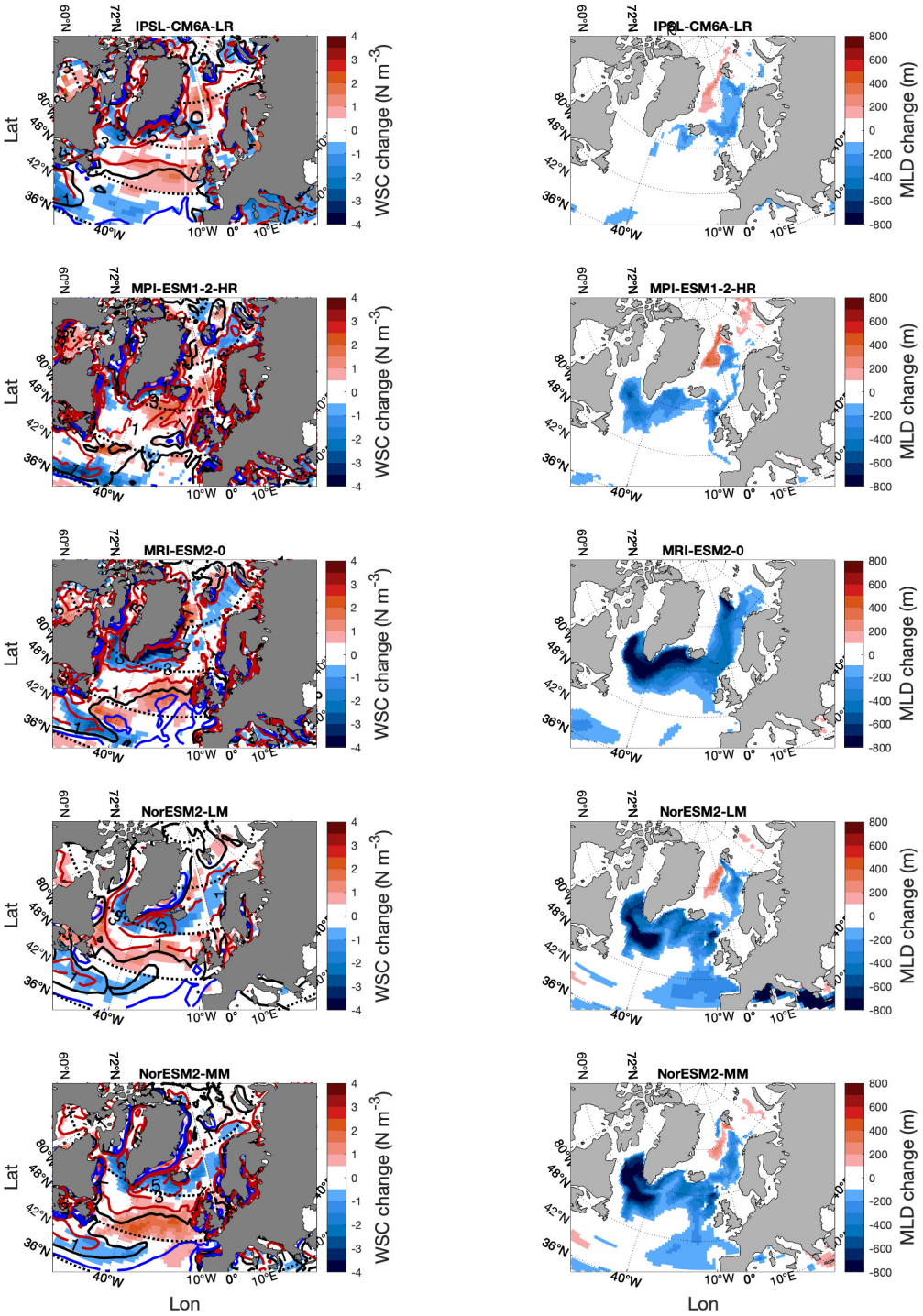


Figure 4: Changes in the wind stress curl (WSC) and mixed layer depth (MLD) for IPSL-CM6A-LR, MPI-ESM1-2-HR, MRI-ESM2-0, NorESM2-LM and NorESM2-MM (top-down) during the SSP5-8.5 scenario (2015-2100). Both indicators are calculated as means of January-March when both winds and mixed layer depths are generally at their maximum (Meccia *et al.*, 2021). The contours in the panel to the left show the average position of the positive (red), negative (blue) and zero (black) WSC during the first 20 years of the scenario (present time). The WSC is multiplied by 10^7.

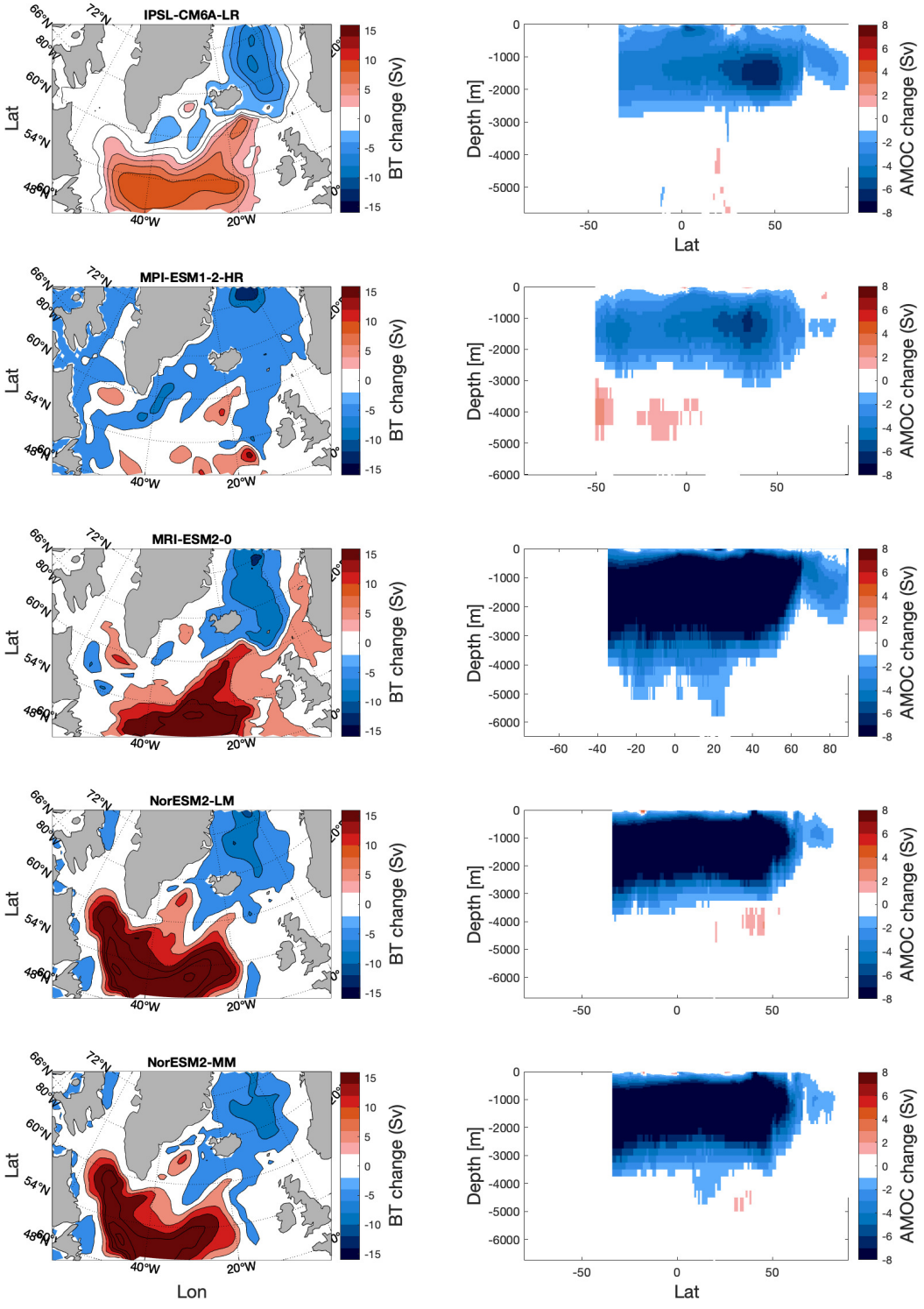


Figure 5: Changes in the barotropic stream function (BT) (Sv, left), and changes in the Atlantic meridional overturning circulation (AMOC) (Sv, right) for IPSL-CM6A-LR, MPI-ESM1-2-HR, MRI-ESM2-0, NorESM2-LM and NorESM2-MM (top-down) during the SSP5-8.5 scenario (2015-2100). Note that that the BT change of IPSL-CM6A-LR has been reduced overall by a constant value of 15 Sv to be visually comparable to the other models.

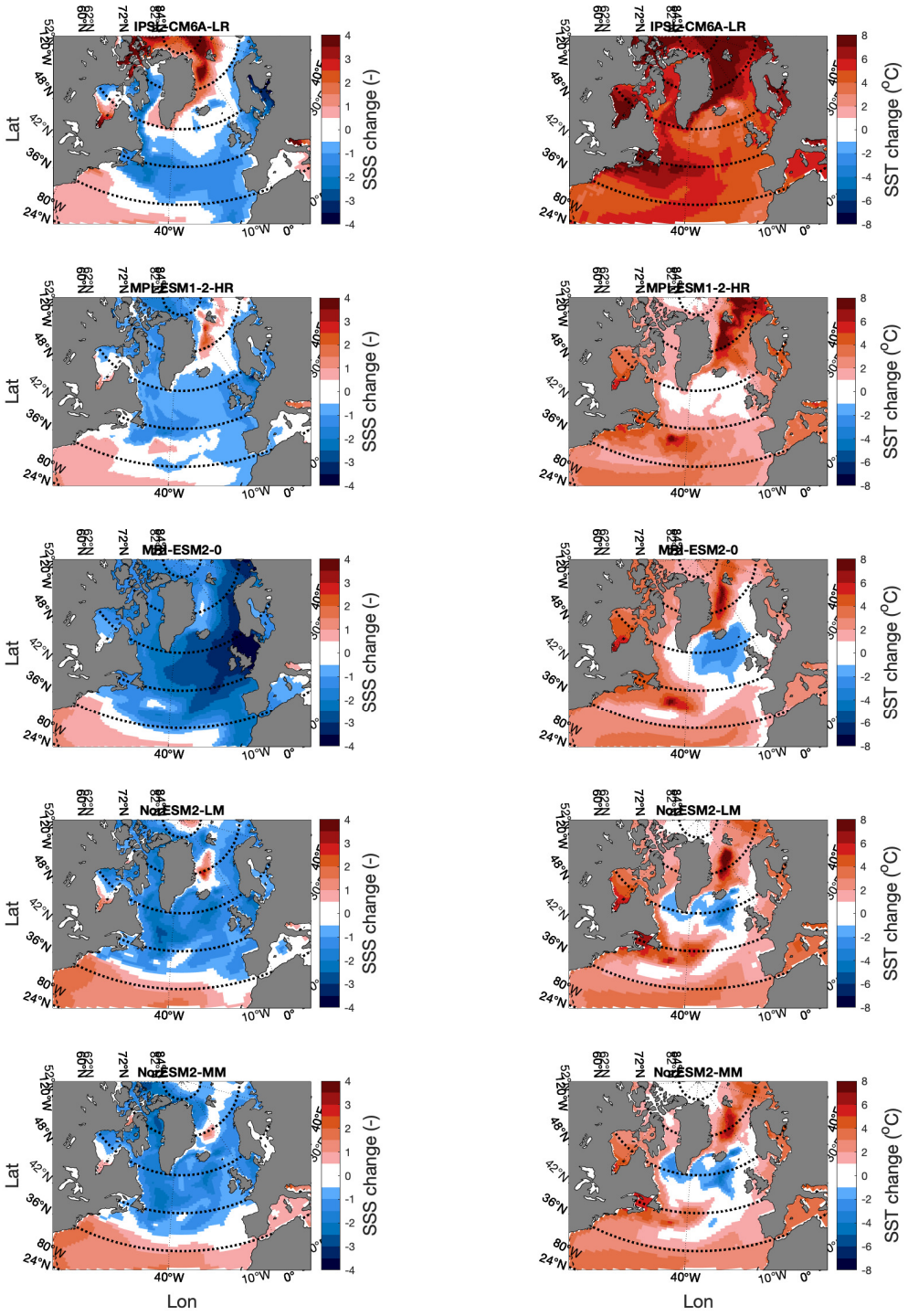


Figure 6: Changes in the sea surface salinity (SSS) and sea surface temperature (SST) for IPSL-CM6A-LR, MPI-ESM1-2-HR, MRI-ESM2-0, NorESM2-LM and NorESM2-MM (top-down) during the SSP5-8.5 scenario (2015-2100).

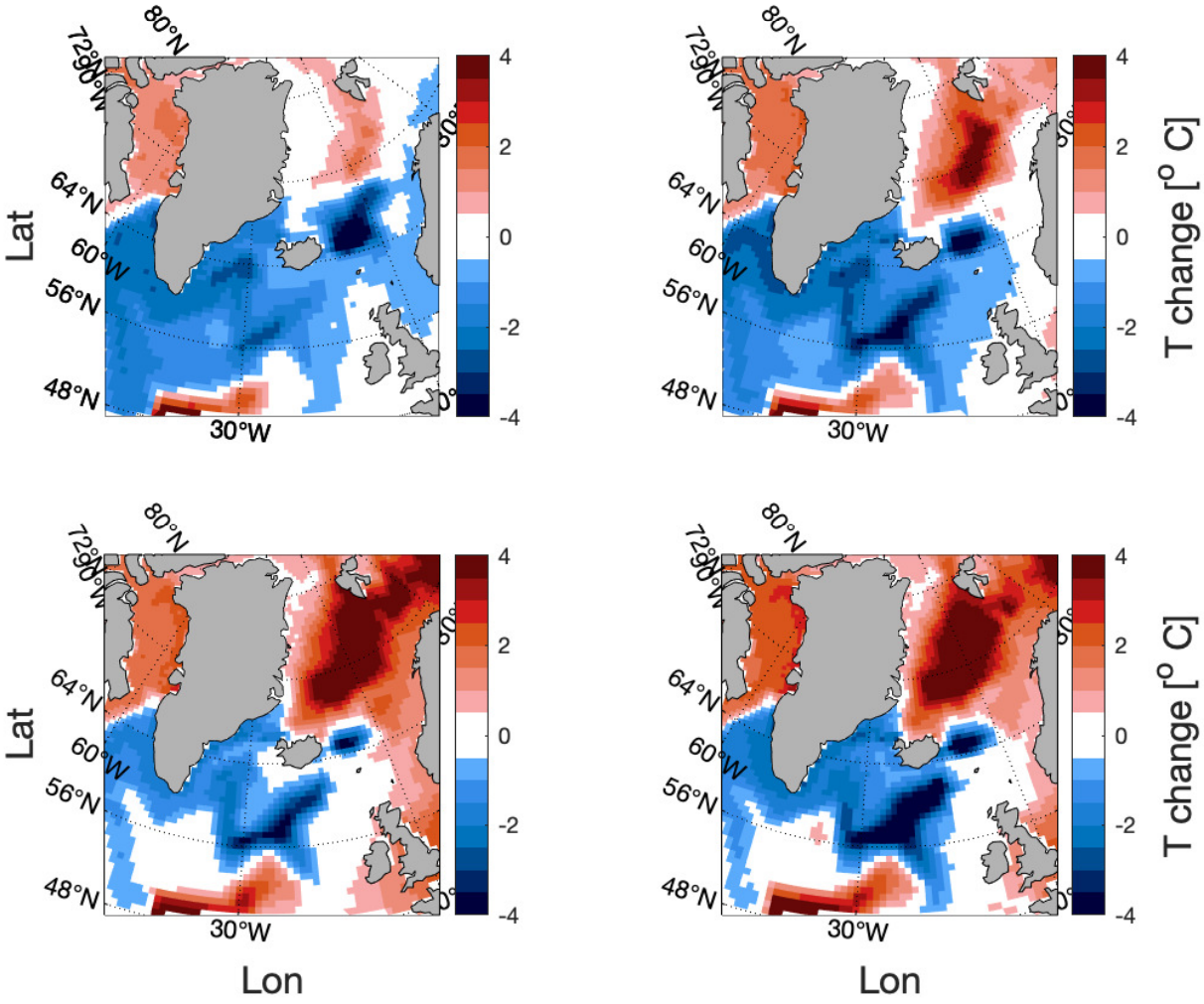


Figure 7: Spatial changes in the mean temperature at 0-200m (°C, right) in NorESM2-MM scenarios SSP1-2.6 (upper left), SSP2-4.5 (upper right), SSP3-7.0 (lower left) and SSP5-8.5 (lower right) between 2015 and 2100.

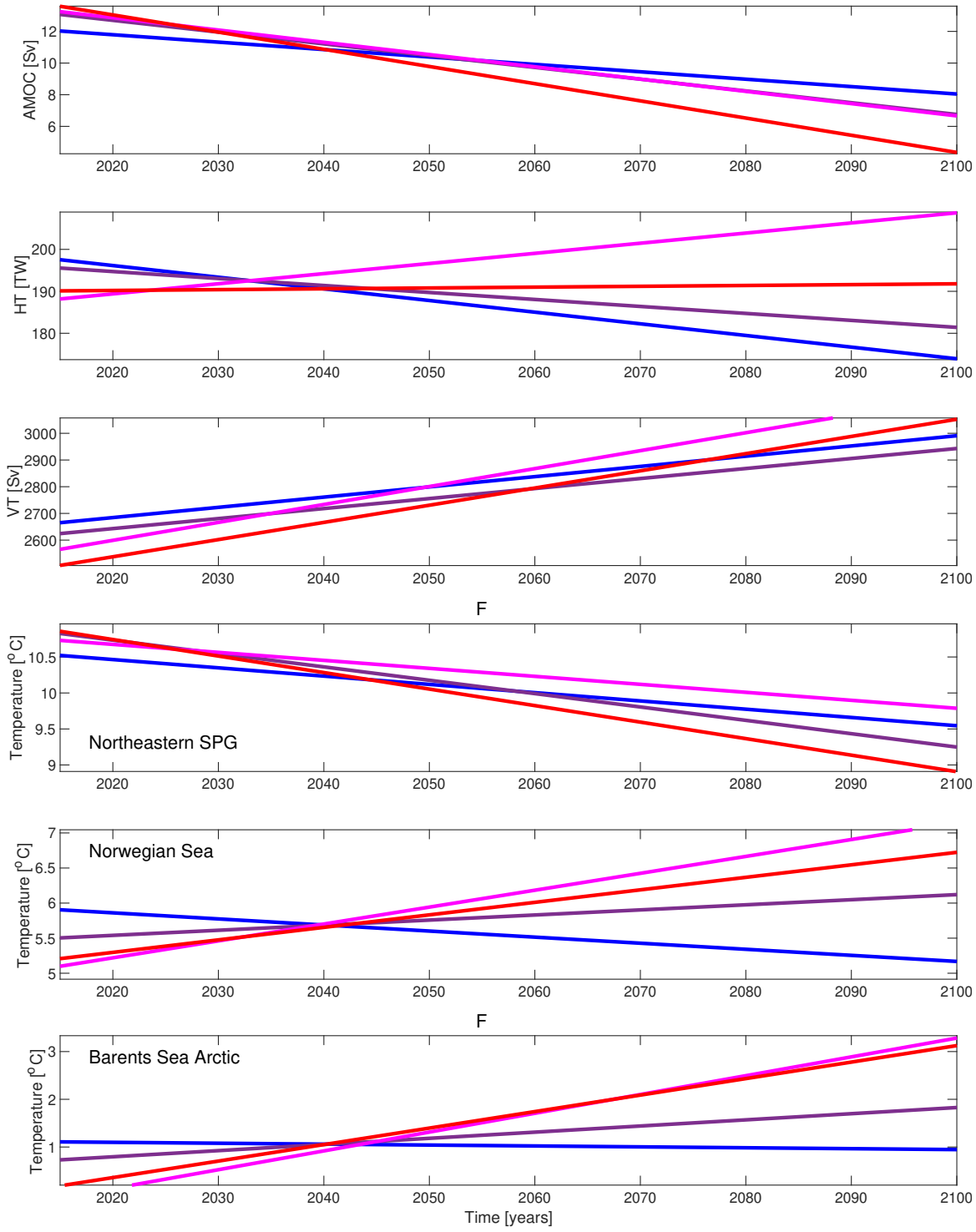


Figure 8: Trends for AMOC (Sv), HT (TW), VT (Sv) and mean temperature at 0-200m (°C) in Northeastern SPG (59-63° N, 28-80° W), Norwegian Sea and Barents Sea Arctic (regions defined in Sandø *et al.* (2024)) (top-down) from the NorESM2-MM scenarios SSP1-2.6 (blue), SSP2-4.5 (purple), SSP3-7.0 (magenta) and SSP5-8.5 (red) between 2015 and 2100.